

## Research Article

Cindyawati Cindyawati, Faozan Ahmad, Hendradi Hardhienata, Agus Kartono\*

# Development of A $\beta$ and anti-A $\beta$ dynamics models for Alzheimer's disease

<https://doi.org/10.1515/cmb-2024-0008>

received January 27, 2024; accepted July 14, 2024

**Abstract:** Alzheimer's disease is one of the most prevalent types of dementia worldwide. It is caused by the accumulation of amyloid-beta (A $\beta$ ) plaques in the brain, disrupting communication pathways and memory. Microglia and astrocytes act as the immune system of the brain, clearing A $\beta$  plaque deposits. However, these cells can lose effectiveness when A $\beta$  plaque accumulation exceeds normal limits, leading to inflammation induced by proinflammatory cytokines. One type of treatment involves anti-A $\beta$  drug therapy. Anti-A $\beta$  drugs are believed to have the ability to reduce A $\beta$  plaque deposits effectively. The mechanism of A $\beta$  plaque accumulation can be explained by ordinary differential equations describing the growth of A $\beta$  monomers. In this study, we aimed to develop a new mathematical model to elucidate the role of the immune system and drug therapy in reducing A $\beta$  plaque deposits. Based on the simulation results, we conclude that the use of anti-A $\beta$  drug therapy can decrease the concentration of A $\beta$  plaque deposits, and the effective treatment duration for Alzheimer's patients is estimated to be approximately 4 months starting from the time the drug was first administered.

**Keywords:** Alzheimer, amyloid-beta (A $\beta$ ), drug therapy, immune system, ordinary differential equation

**MSC 2020:** 34A12, 92-08, 92-10

## 1 Introduction

Dementia is a type of disease that affects the nervous system and causes memory loss [5]. The most common type of dementia is Alzheimer's disease, accounting for approximately 60–80% of cases [42]. Generally, individuals aged 65 years and older with Alzheimer's disease, especially women, are more susceptible to this disease [14]. Alzheimer's disease accounts for only 4–6% of deaths. According to information from Statista and the Alzheimer's Association, approximately 37 out of 100 thousand people, or approximately 0.037%, died due to Alzheimer's disease from 2000 to 2019 [11]. However, the number of Alzheimer's sufferers worldwide reached 47 million in 2016, and this figure is expected to continue to increase to 131 million by 2050 [10]. The estimated cost to Alzheimer's patients worldwide is approximately US\$818 billion [7]. Therefore, Alzheimer's

---

\* **Corresponding author: Agus Kartono**, Department of Physics, Faculty of Mathematical and Natural Science, IPB University (Bogor Agricultural University), Jalan Meranti, Building Wing S, 2nd Floor, Kampus IPB Dramaga, Bogor, 16680, Indonesia, e-mail: akartono@apps.ipb.ac.id

**Cindyawati Cindyawati:** Department of Physics, Faculty of Mathematical and Natural Science, IPB University (Bogor Agricultural University), Jalan Meranti, Building Wing S, 2nd Floor, Kampus IPB Dramaga, Bogor, 16680, Indonesia, e-mail: cindyaaa77@gmail.com

**Faozan Ahmad:** Department of Physics, Faculty of Mathematical and Natural Science, IPB University (Bogor Agricultural University), Jalan Meranti, Building Wing S, 2nd Floor, Kampus IPB Dramaga, Bogor, 16680, Indonesia, e-mail: faozan@apps.ipb.ac.id

**Hendradi Hardhienata:** Department of Physics, Faculty of Mathematical and Natural Science, IPB University (Bogor Agricultural University), Jalan Meranti, Building Wing S, 2nd Floor, Kampus IPB Dramaga, Bogor, 16680, Indonesia, e-mail: hendradi@apps.ipb.ac.id  
ORCID: Faozan Ahmad 0000-0001-6182-0780; Hendradi Hardhienata 0000-0001-9123-4539; Agus Kartono 0000-0002-4081-5795

disease patients require special care because the management of this disease has social and economic implications.

One of the causes of Alzheimer's disease is the accumulation of A $\beta$  plaques in the hippocampus. In Alzheimer's disease patients, the hippocampus undergoes atrophy, leading to difficulties in processing and transmitting memories [8]. Amyloid precursor protein (APP) cleavage mistakes result in misfolding of the A $\beta$  monomer, which leads to the formation of A $\beta$  plaques. APP undergoes two crucial processes: nonamyloidogenic and amyloidogenic processes. Under normal conditions, APP undergoes a nonamyloidogenic process, in which it is cleaved by  $\alpha$ -secretase and  $\gamma$ -secretase to produce soluble sAPP- $\alpha$  and p3 in the cerebrospinal fluid. Conversely, under abnormal conditions, APP undergoes the amyloidogenic process, where it is cleaved by  $\beta$ -secretase and  $\gamma$ -secretase, resulting in soluble sAPP- $\beta$  and non-soluble monomer A $\beta$  in the brain [20,26]. A $\beta$  monomers accumulate to form oligomers and eventually form fibrils. Fibril stacks precipitate and eventually form toxic plaques [8].

The A $\beta$  aggregation process is divided into two phases: nucleation and elongation [12,15]. Thermodynamically, the nucleation phase requires more energy than the elongation phase. This is because, in contrast to the elongation phase, the nucleation phase develops more slowly and involves the production of A $\beta$  monomers ( $M_1$ ) into dimers ( $M_2$ ), trimers ( $M_3$ ), tetramers ( $M_4$ ), and ultimately oligomers ( $O$ ). On the other hand, the elongation phase requires less energy. This is because the elongation phase involves the process of adding length to oligomers ( $O$ ) to form fibrils ( $P$ ), and it proceeds more quickly [5].

Astrocytes and microglia are immune systems present in the brain. In Alzheimer's patients, the main trigger for the activation of microglia and astrocytes is the accumulation of A $\beta$ . Microglia, which function like macrophages, play a role in clearing A $\beta$  deposits. This process causes microglia to enlarge, gradually reducing their functional capacity over time. This decline in function reduces the ability to break down A $\beta$  plaques, leading to the accumulation of A $\beta$  and the production of proinflammatory cytokines that can damage neurons [4]. Astrocytes function to repair nerve injuries and play a role in neurotransmitter activity. Tumor necrosis factor alpha (TNF- $\alpha$ ) is a cytokine that affects astrocyte activation. It automatically causes the production of monocyte chemoattractant protein 1 (MCP-1). MCP-1 attracts monocytes from the blood into plaques. When danger is detected, monocytes differentiate into macrophages. Macrophages are divided into proinflammatory ( $M_{a\pi}$ ) and anti-inflammatory ( $M_{ai}$ ) types. Activated microglia have two phenotypes: proinflammatory microglia ( $M_{i\pi}$ ) and anti-inflammatory microglia ( $M_{iai}$ ) [42]. Nerve damage is exacerbated by toxic  $M_{i\pi}$  and  $M_{a\pi}$  which produce TNF- $\alpha$ , IL-6, IL-12, and IL-1 $\beta$ , while  $M_{ai}$  and  $M_{iai}$  produce anti-inflammatory IL-10, IL-13, IL-4, and TGF- $\beta$  to counteract proinflammation [14]. The immune system is suspected to contribute to the development of Alzheimer's disease, but the extent of the immune system's role in Alzheimer's disease still needs to be studied [11].

Research on A $\beta$  plaque accumulation as one of the causes of Alzheimer's disease is continually being conducted, both through experiments and simulations. Numerous mathematical models have been applied, primarily aiming to understand the mechanism of A $\beta$  plaque growth. Current medications can only reduce A $\beta$  plaque deposits, and treatment duration plays a crucial role in recovery. Simulation models of A $\beta$  dynamics aim to predict A $\beta$  growth to determine an effective treatment duration. Therefore, this research aimed to simulate the biological dynamics of A $\beta$  growth, the interaction between the immune system and the use of anti-A $\beta$  drug therapy.

Mathematical models serve as effective tools to test hypotheses and confirm experiments using dynamic simulations. Through these models, we can manipulate the mechanisms of biological dynamic systems in a relatively short time without risking extensive laboratory trial periods. Variations in biological system dynamics models can be adjusted to match the experiments under consideration. In Alzheimer's disease dynamic simulations, models can be validated using clinical experimental information, although clinical experiments are still rare. Therefore, simulation results can be used as hypotheses for Alzheimer's disease development, considering treatment durations. Quantitative models have been developed as an experimental approach to Alzheimer's disease. These models are typically formulated as ordinary differential equations based on A $\beta$  concentrations, opening avenues for research in Alzheimer's disease modeling. As this research can enhance Alzheimer's disease treatment models, the models can be utilized to determine effective treatment durations.

Craft et al. [8] formulated and analyzed a mathematical model for A $\beta$  aggregation from a monomeric form to a fibril. Because the model is written in coupled differential equations, the mechanism by which monomers grow into fibrils and eventually form plaques can be examined. The models they outlined rely on both continuous-time and dynamic-time models. Their simulation results indicate that the concentration of A $\beta$  aggregates is influenced by parameters involved in monomer production during the nucleation phase, emphasizing the need for accurate parameter value estimates.

Hao and Friedman [14] developed a mathematical model of Alzheimer's disease that incorporates the roles of microglia and astrocytes. The model is expressed in partial differential equations. The role of the immune system in clearing A $\beta$  plaque deposits can be analyzed, making it applicable for simulating the effects of the most effective drugs.

Currently, drug development research is ongoing both *in silico* and *in vivo*. Some examples of potential drugs are Etanercept, Bindarit, and Aducanumab [14]. Aducanumab is a type of anti-A $\beta$  drug that functions as a monoclonal immune system. This drug is designed to target and bind to accumulated A $\beta$ . According to data from the Drug Bank, Aducanumab successfully received approval from the Food and Drug Administration as the first Alzheimer's therapy drug in 2021 [10]. Aducanumab works selectively by binding to A $\beta$  oligomers and fibrils rather than in a monomeric form. This distinction distinguishes Aducanumab from other anti-A $\beta$  drugs.

Thus, to track the development of A $\beta$  concentrations, we will create a mathematical model in this study that will be used for studies of the immune system and anti-A $\beta$  medication. The results of developing this model are expected to provide insights into effective treatment durations and the future development of drug manufacturing.

This research will present the development of a mathematical model describing the growth of A $\beta$  monomers into fibrils, interactions with the immune system, and anti-A $\beta$  drug therapy. The article consists of three sections. Section 2 presents the development of the mathematical model and the detailed values of the model parameters used. Section 3 provides the results and analysis of the simulations conducted. Finally, Section 4 presents the conclusion.

## 2 Formulation of mathematical models of combination therapy

### 2.1 Mathematical model of the growth of A $\beta$

This research began with developing a model based on equations proposed by Craft et al. [8]. The A $\beta$  aggregation process is modeled by selecting the nucleation phase, where the process occurs more slowly. This makes it possible to consider the concentrations of monomer ( $M_1$ ), dimer ( $M_2$ ), trimer ( $M_3$ ), and so on. The next process builds oligomer ( $O$ ) and fibril ( $P$ ) models by considering them as the average values of  $O$  and  $P$ .

The first assumption is that an oligomer forms at least  $n + 1$  monomers, resulting in an equation containing  $n + 2$  components, namely, monomers ( $M_1$ ), dimers ( $M_2$ ), trimers ( $M_3$ ), ...,  $M_n$ , oligomers ( $O$ ), and fibrils ( $P$ ). The second assumption is that aggregation occurs through the addition of monomers. To simplify the model, the separation of monomers from aggregates is not considered. This is because the separation process is slower than the aggregation process. The above assumptions can be expressed in the following equations:

$$\begin{aligned}
 M_1 + M_1 &= 2M_1 \rightarrow M_2 \\
 M_1 + M_2 &\rightarrow M_3 \\
 M_1 + M_3 &\rightarrow M_4 \\
 &\vdots \\
 M_1 + M_{n-1} &\rightarrow M_n \\
 (O_a - n)M_1 + M_n &\rightarrow O \\
 (P_a - O_a)M_1 + O &\rightarrow P,
 \end{aligned} \tag{1}$$

where  $O_a$  and  $P_a$  are the average sizes of the oligomers and fibrils, respectively. The above equation describes the primary nucleation process with the assumption that the number of monomers composing the aggregate is stable.

Because monomers are produced in the brain, the third assumption is that the production process can be represented by the saturation function  $f(M_1)M_1$ , where  $f(M_1)M_1 = \delta M_1 \left(1 - \frac{M_1}{\gamma}\right)$  with  $\delta$  indicating the average growth of monomers and  $\gamma$  indicating the carrying capacity. The choice of this function is because the concentration of monomers cannot increase into larger structures if the monomers are not bound to each other. This function selection applies to the general case of a nonlinear  $f(M_1)$  that satisfies the conditions  $f(0) = \delta > 0$  and  $f'(M_1) < 0$ . The fourth assumption is the existence of A $\beta$  stack clearance denoted as  $\mu_i$ .

Explanation of the assumptions used in the simulation model:

1. **Oligomer formation:** The formation of oligomers begins stepwise from monomers ( $M_1$ ), dimers ( $M_2$ ), trimers ( $M_3$ ), and so on, consisting of at least  $n + 1$  monomers. The entire process involves  $n + 2$  components, including monomers, dimers, trimers, and oligomers. This assumption is used to explain the components involved in the molecular aggregation process from single monomers to the formation of larger structures such as oligomers and fibrils.
2. **Aggregation process:** The aggregation into larger structures occurs through the gradual addition of monomers, such as the first monomer joining with the second to form a dimer. This dimer can then add a third monomer to form a trimer, and so on.
3. **Monomer production rate:** The third assumption indicates that the rate of monomer production depends on the concentration of the monomers themselves, meaning there is an initial rapid growth when the monomer concentration is low, but the growth rate slows down and eventually stops when the maximum capacity is reached.
4. **Degradation factor ( $\mu_i$ ):** The degradation factor ( $\mu_i$ ) indicates that there is a mechanism for clearing A $\beta$  stacks during the growth of A $\beta$ . This assumption is important to describe the dynamic balance between the formation and clearance of A $\beta$  stacks in the system.

Meanwhile, the assumptions used can be written in the following differential equations:

$$\begin{aligned} \frac{dM_1(t)}{dt} &= \delta M_1(t) \left(1 - \frac{M_1(t)}{\gamma}\right) - 2K_1 M_1^2(t) - M_1(t) \sum_{i=2}^{n-1} K_i M_i(t) - (O_a - n)K_n M_1(t)M_n(t) \\ &\quad - (P_a - O_a)K_o M_1(t)O(t) - \mu_1 M_1(t), \\ \boxed{\frac{dM_2(t)}{dt} = K_1 M_1^2(t) - K_2 M_1(t)M_2(t) - \mu_2 M_2(t)} &\rightarrow \text{We refer the eq as GA}\beta \\ &\quad \vdots \text{ (Growth of A}\beta\text{)} \\ \frac{dM_n(t)}{dt} &= K_{n-1} M_1(t)M_{n-1}(t) - K_n M_1(t)M_n(t) - \mu_n M_n(t) \\ \frac{dO(t)}{dt} &= K_n M_1(t)M_n(t) - K_o M_1(t)O(t) - \mu_o O(t) \\ \frac{dP(t)}{dt} &= K_o M_1(t)O(t) - \mu_p P(t). \end{aligned} \quad (2)$$

The factors  $(O_a - n)$  and  $(P_a - O_a)$  in each monomer equation represent the average number of monomers that need to be added to the aggregate  $M_n$  to form an oligomer and the average number of monomers that need to be added to the oligomer to form a fibril, respectively. Both factors are added to ensure the conservation of mass.

The selection of initial conditions and parameter values is crucial in the development of the Alzheimer's dynamic model because it can influence the simulation results. Equation (3) indicates the parameter values and initial conditions used in the simulation.

$$\begin{aligned}
n &= 6, \delta = 50, \gamma = 75, K_1 = 10^{-4}, K_2 = 5 \times 10^{-4}, K_3 = 10^{-3}, \\
K_4 &= 5 \times 10^{-3}, K_5 = 10^{-2}, K_6 = 5 \times 10^{-2}, K_O = 0.1, \\
O_a &= 10, P_a = 100, \mu_1, \mu_2 \cdots \mu_6 = 10^{-3}, \mu_O = 10^{-4}, \mu_P = 10^{-5} \\
M_1 &= 10, M_2 \cdots M_6 = O = P = 0.
\end{aligned} \tag{3}$$

Naturally, the parameters involved in the A $\beta$  aggregation process have a very wide range of values. Based on this, the values of  $K_1$  until  $K_6$  in Table 1 are determined to illustrate the aggregation growth curve of A $\beta$ . However, the values of  $K_1$ – $K_6$  in Table 1 may not represent the actual process values. The illustrative curve of the A $\beta$  aggregation growth process is formed to understand the growth pattern of A $\beta$ .

The estimation of the parameter  $K_O$  given in Table 1 is based on the addition of one monomer ( $M_1$ ) because the  $K_O$  elongation rate in this model involves the addition of  $P_a - O_a$  monomers. We modified this estimate based on the relative sizes of fibrils and oligomers ( $O$ ) [7,8,26]. The estimation of  $O_a$  and  $P_a$  values is based on studies of monomer binding characteristics up to fibril formation.

The degradation rate ( $\mu_n$ ) depends on the size of the molecule. The larger the size, the slower the degradation rate. Based on this, the degradation value is chosen from the relative size ratio between monomers ( $M_1$ ) and fibrils ( $P$ ) [8,14].

In the initial condition, the value of  $\delta$  is chosen to be 50 because it would represent the level of aggregation or polymerization of A $\beta$  monomers into oligomers or fibrils, which is influenced by monomer concentration. The value of  $\gamma$  is set to 75 because the intracellular transport system is assumed to be efficient enough to move A $\beta$  monomers from one location to another. The value  $n = 6$  is selected because the minimum formation to become an oligomer is  $n = 5$  or more.  $M_1$  is valued at 10 because it would represent the initial concentration for the A $\beta$  growth process. For  $M_2$  until  $P$ , the initial value of concentration is set to zero as these molecules are yet to be produced.

**Table 1:** Description and parameter estimation values based on reference for the A $\beta$  aggregation model for equations (2) and (3)

Parameter	Description	Value	Reference
$K_1 - K_6$	Nucleation rate	$10^{-6} - 10^{-4} \text{ M}^{-1}\text{s}^{-1}$	[7,20]
$K_O$	Elongation rate	$10^{-1} - 10^4 \text{ M}^{-1}\text{s}^{-1}$	[7,8,20,26]
$O_a$	Average oligomer size	2 – 10	[12,15,24]
$P_a$	Average fibril size	$10 - 10^3$	[26]
$\mu_1 - \mu_6$	Degradation rate of monomers	$10^{-5} - 10^{-3} \text{ s}^{-1}$	[8,14]
$\mu_O$	Degradation rate of oligomers	$10^{-6} - 10^{-4} \text{ s}^{-1}$	[14]
$\mu_P$	Degradation rate of fibrils	$10^{-7} - 10^{-5} \text{ s}^{-1}$	Estimated

## 2.2 Mathematical model of the immune system

Hao and Friedman [14] developed a mathematical model for the role of microglia and astrocytes in Alzheimer's disease. There are two phenotypes of active microglia: proinflammatory ( $M_{ipi}$ ) and anti-inflammatory ( $M_{iai}$ ) phenotypes.

The equation for the immune system includes proinflammatory ( $M_{ipi}$ ) and anti-inflammatory ( $M_{iai}$ ) microglia can be written as follows:

$$\begin{aligned}
\frac{dM_{ipi}}{dt} &= M_G^0 \left[ \frac{\lambda_{MF}F_O}{F_O + KF_O} + \frac{\lambda_{MA}A_O}{A_O + KA_O} \right] \frac{\beta\epsilon_1}{\beta\epsilon_1 + \epsilon_2} - \underbrace{\frac{\lambda_{M_{ipi}T_\beta}T_\beta M_{ipi}}{T_\beta + KT_\beta}}_{M_{ipi} \rightarrow M_{iai}} - \underbrace{d_{M_{ipi}}M_{ipi}}_{\text{Death of Microglia}} \rightarrow \text{We refer the equation as MIP (Microglia Proinflammatory)} \\
\frac{dM_{iai}}{dt} &= M_G^0 \left[ \frac{\lambda_{MF}F_O}{F_O + KF_O} + \frac{\lambda_{MA}A_O}{A_O + KA_O} \right] \frac{\epsilon_2}{\beta\epsilon_1 + \epsilon_2} + \underbrace{\frac{\lambda_{M_{ipi}T_\beta}T_\beta M_{ipi}}{T_\beta + KT_\beta}}_{M_{ipi} \rightarrow M_{iai}} - \underbrace{d_{M_{iai}}M_{iai}}_{\text{Death of Microglia}} \rightarrow \text{We refer the equation as MIA (Microglia Anti-inflammatory)}
\end{aligned} \tag{4}$$

So, the model of the immune system can be written as follows:

$$\text{Model of Immune System (MIS)} = \text{MIP} + \text{MIA}, \quad (5)$$

where  $\varepsilon_1 = \frac{T_a}{T_a + K_{Ta}}$ ,  $\varepsilon_2 = \frac{I_{10}}{I_{10} + K_{I10}}$ , and  $\frac{\beta\varepsilon_1}{\beta\varepsilon_1 + \varepsilon_2}$  indicate the ratio of microglia becoming  $M_{a\text{pi}}$  macrophages, and  $\frac{\varepsilon_2}{\beta\varepsilon_1 + \varepsilon_2}$  indicates the ratio of microglia becoming  $M_{a\text{ai}}$  macrophages. The phenotype  $M_{i\text{pi}}$  is under the control of TNF- $\alpha$  and  $M_{i\text{ai}}$  is under the control of IL-10. Table 2 shows the parameter values used by microglia as the immune system in the brain.

**Table 2:** Description and estimated parameter values based on references for the role of the immune system models for equation (4)

Parameter	Description	Value	Reference
$M_G^0$	Concentration of microglia	0.047 g mL <sup>-1</sup>	
$\lambda_{MF}$	Activation rate of microglia by neurofibrillary tangles (NFT)	$5 \times 10^{-2}$ day <sup>-1</sup>	
$F_O$	Concentration of NFT outside neurons	$3.36 \times 10^{-5}$ g mL <sup>-1</sup>	
$K_{FO}$	Average concentration of extracellular NFT	$2.58 \times 10^{-5}$ g mL <sup>-1</sup>	
$\lambda_{MA}$	Activation rate of microglia by astrocytes	$2.23 \times 10^{-2}$ day <sup>-1</sup>	
$A_O$	Density of astrocytes outside neurons	0.140 g mL <sup>-1</sup>	
$K_{AO}$	Average concentration of oligomer A $\beta$	$10^{-7}$ g mL <sup>-1</sup>	
$\beta$	Proinflammatory/anti-inflammatory ratio	10	
$\varepsilon_1$	Ratio of TNF- $\alpha$ to half-life of TNF- $\alpha$	0.333	[14]
$\varepsilon_2$	Ratio of IL-10 to half-life of IL-10	0.800	
$\lambda_{M_{i\text{pi}}T\beta}$	Rate of $M_{i\text{pi}} \rightarrow M_{i\text{ai}}$	$6 \times 10^{-3}$ day <sup>-1</sup>	
$T_\beta$	Value of TGF- $\beta$	$10^{-6}$ g mL <sup>-1</sup>	
$K_{T\beta}$	Half-life of TGF- $\beta$	$2.5 \times 10^{-7}$ g mL <sup>-1</sup>	
$M_{i\text{pi}}, M_{i\text{ai}}$	Value of proinflammatory and anti-inflammatory microglia	0.020 g mL <sup>-1</sup>	
$K_{Ta}$	Half-life of TNF- $\alpha$	$4 \times 10^{-5}$ g mL <sup>-1</sup>	
$I_{10}$	Value of IL-10	$10^{-5}$ g mL <sup>-1</sup>	
$K_{I10}$	Half-life of IL-10	$2.5 \times 10^{-6}$ g mL <sup>-1</sup>	

## 2.3 Mathematical model of drug therapy

Hao and Friedman [14] developed a mathematical model for the use of Alzheimer's drug therapy. One of the drugs used is Aducanumab. Aducanumab is chosen as an anti-A $\beta$  agent. The use of anti-A $\beta$  drugs can be described by the below equation:

$$\frac{dA_\beta^o}{dt} = A_\beta^i \left| \frac{dN}{dt} \right| + \lambda_N \frac{N}{N_0} + \lambda_A \frac{A}{A_0} - (d_{A_\beta M_a}^o (M_{a\text{pi}} + \theta M_{a\text{ai}}) + d_{A_\beta M_i}^o (M_{i\text{pi}} + \theta M_{i\text{ai}})(1 + h)) \frac{A_\beta^o}{A_\beta^o + \bar{K}_{A_\beta}^o}, \quad \rightarrow \quad \begin{array}{l} \text{We refer the eq as DA}\beta \\ \text{(Drug A}\beta\text{)} \end{array} \quad (6)$$

The parameter  $h$  represents the dosage of the drug, and the value is 10. We used 10 because based on the clinical test of the drug.  $N$  represents the number of live neurons,  $N_0$  is the mass density of neurons,  $A$  represents astrocytes, and  $A_0$  represents the mass density of astrocytes, with the values used for all parameters being 0.14 g mL<sup>-1</sup> (Table 3).

**Table 3:** Description and parameter estimation values based on reference for the drug therapy models for equation (6)

Parameter	Description	Value	Reference
$A_{\beta}^i$	Concentration of A $\beta$ inside neurons	$10^{-6}$ g mL $^{-1}$	
$A_{\beta}^o$	Concentration of A $\beta$ outside neurons	$10^{-8}$ g mL $^{-1}$	
$\lambda_N$	Production rate of $A_{\beta}^o$ by neurons	$8 \times 10^{-4}$ g mL $^{-1}$ day $^{-1}$	
$\lambda_A$	Production rate of $A_{\beta}^o$ by astrocytes	$8 \times 10^{-4}$ g mL $^{-1}$ day $^{-1}$	
$d_{A_{\beta}M_a}^o$	Clearance rate of $A_{\beta}^o$ by macrophages	$2 \times 10^{-3}$ day $^{-1}$	[14]
$d_{A_{\beta}M_i}^o$	Clearance rate of $A_{\beta}^o$ by microglia	$10^{-2}$ day $^{-1}$	
$M_{a\pi i}, M_{aai}$	Concentration of macrophages proinflammatory and anti-inflammatory	0 g mL $^{-1}$	
$M_{i\pi i}, M_{iai}$	Concentration of microglia proinflammatory and anti-inflammatory	0.020 g mL $^{-1}$	
$\theta$	Ratio effectivity $M_{i\pi i}/M_{iai}$ in clearance of $A_{\beta}^o$	0.9	
$\bar{K}_{A_{\beta}}^o$	Michaelis–Menten coefficient of $A_{\beta}^o$	$7 \times 10^{-3}$ g mL $^{-1}$	

## 2.4 Connection of the model

In this subsection, the integration of the immune system model (2.2) and the drug therapy model (2.3) into the core A $\beta$  growth model (2.1) will be shown. The equations in Sections 2.2 and 2.3 will serve as “modifier” equations for the core model; hence, the A $\beta$  growth would also modified. The modification is performed by incorporating the equations from Sections 2.2 and 2.3 into the equation  $\frac{dM_2(t)}{dt}$  in the A $\beta$  growth model. This modification will affect  $\frac{dM_2(t)}{dt}$  up to  $\frac{dP(t)}{dt}$ . This is because the A $\beta$  growth model equations are coupled differential equations. The reason for modifying only  $\frac{dM_2(t)}{dt}$  is that A $\beta$  monomers ( $M_1$ ) are small in size and non-toxic and thus are not yet detected by the immune system and drugs [8,14].

The results of the modifications to the core A $\beta$  growth model are as follows:

1	Growth of A $\beta$	=	GA $\beta$
2	Modification by the immune system on A $\beta$ growth	=	Growth of the A $\beta$ – model of the immune system = GA $\beta$ – MIS
3	Modification by drugs and the immune system on A $\beta$ growth	=	Modification by the Immune System on the A $\beta$ growth – model of drug therapy = GA $\beta$ – MIS – DA $\beta$

In this study, we aimed to integrate mathematical models derived from equations (5) and (6) into equation (2) to obtain three curves: The role of the immune system, the application of drug therapy combined with the immune system, and a model without both as a control. The simulation results include the concentrations of monomer A $\beta$  transforming into fibrils and a comparison of the concentrations of monomeric A $\beta$  transforming into fibrils in the immune system and drug therapy models over time.

## 3 Results and discussion

The results of the third simulation of model development over a duration of 180 days exhibit a sigmoid curve. This sigmoid curve serves as the initial input for the A $\beta$  accumulation process, as it depicts the concentration of A $\beta$  accumulation as a function of time [4,19].

Based on Figure 1, the sigmoid curve consists of three parts: the lag phase, the exponential phase, and the stationary phase. The lag phase indicates a slow initial growth concentration, the exponential phase indicates a



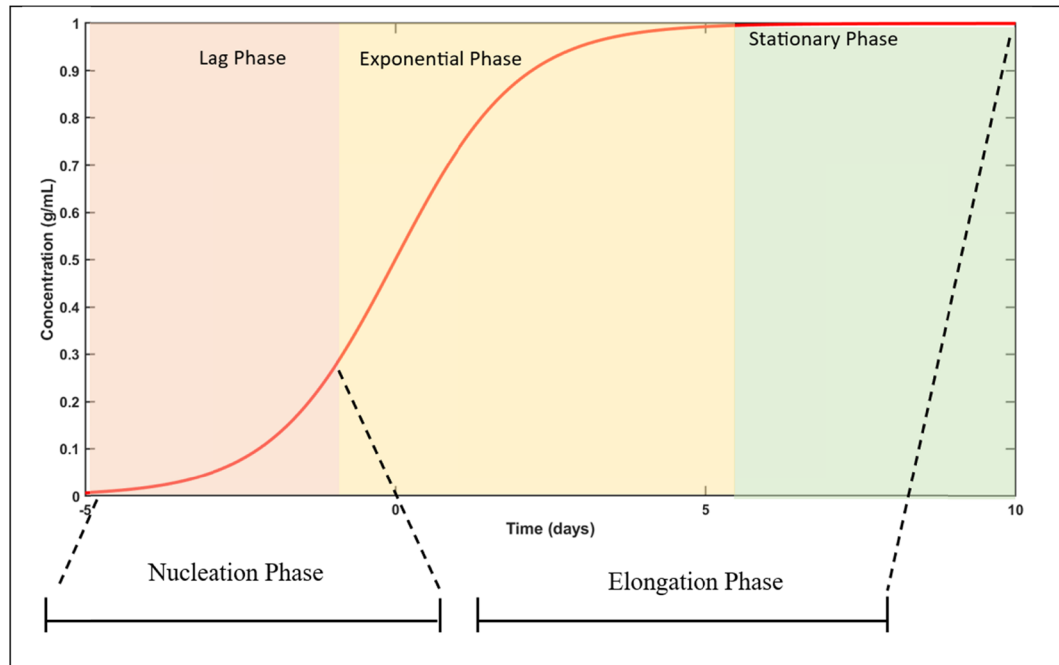


**Figure 1:** The sigmoid curve serves as the initial input, divided into the nucleation phase and the elongation phase.

rapid growth concentration, and the stationary phase indicates a concentration where growth remains unchanged [18]. The nucleation phase begins in the lag phase, where the process involves the formation of monomers until the formation of Aβ oligomers. The elongation phase starts from the exponential phase to the stationary phase, indicating the growth of oligomers into fibrils, ultimately culminating in the formation of Aβ plaques.

The nucleation phase is the starting point in the aggregation process, causing the aggregation process to occur more slowly than the elongation phase. This is because the nucleation phase is the initial process, requiring a significant amount of energy and being thermodynamically unfavorable. Conversely, in the elongation phase, the aggregation process is slightly faster because it is thermodynamically more favorable and requires less energy [5].

### 3.1 Simulation results of the growth of Aβ

The simulation results show the concentration growth of Aβ over time, from the monomeric form ( $M_1$ ) to the fibrils form ( $P$ ), as depicted in Figure 2. Figure 2 shows that the concentration of Aβ increased from  $M_1$  to  $P$ . The  $M_1$  curve indicates that on day 0, the monomer already had a high concentration of  $73.8 \text{ gmL}^{-1}$ . This is attributed to the kinetics of Aβ aggregation. The transition of Aβ monomers to dimers ( $M_2$ ), trimers ( $M_3$ ), tetramers ( $M_4$ ),  $M_5$ ,  $M_6$ , oligomers ( $O$ ), and fibrils ( $P$ ) can occur within a specific concentration range. From day 0 until day 180, the concentration of Aβ monomers remained constant. This finding indicates the relationship between Aβ production and degradation processes. These processes may lead to kinetic dynamics resulting in a constant concentration of Aβ monomers over a specific period. If the concentration of Aβ produced exceeds the degradation capacity, aggregation by Aβ monomers will occur. Aβ monomers join to form dimers, trimers, tetramers, oligomers, and fibrils. As a result, there will be an equilibrium between soluble monomers and aggregated forms.



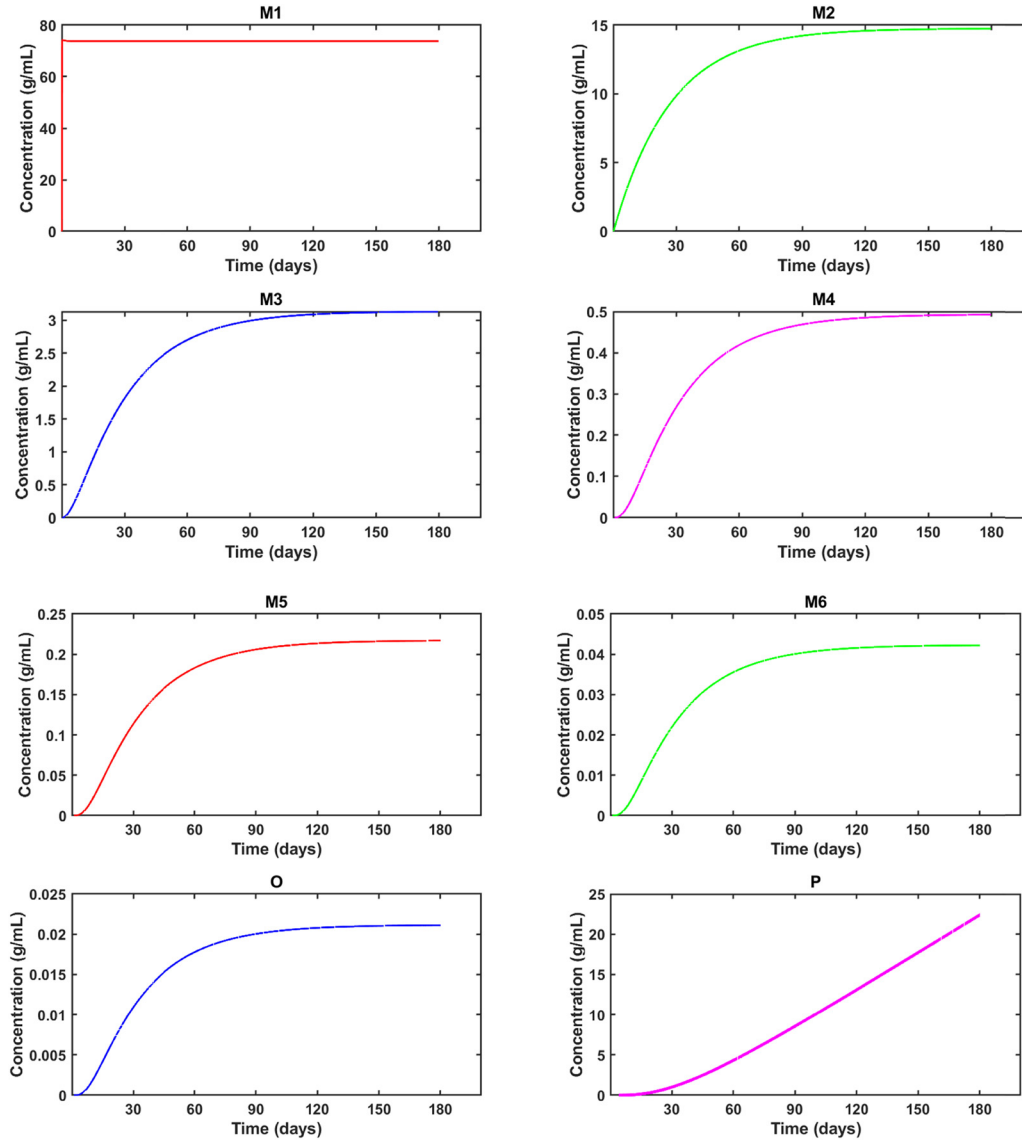


**Figure 2:** The A $\beta$  growth concentrations ( $\text{g mL}^{-1}$ ) for  $M_1$ ,  $M_2$ ,  $M_3$ ,  $M_4$ ,  $M_5$ ,  $M_6$ ,  $O$ , and  $P$  over 180 days (red line =  $M_1$  and  $M_5$ , green line =  $M_2$  and  $M_6$ , blue line =  $M_3$  and  $O$ , and magenta line =  $M_4$  and  $P$ ).

The laws of thermodynamics state that the Gibbs free energy will reach a minimum value. In this case, the equilibrium between A $\beta$  monomers and aggregates results from the lowest change in free energy [3,34,44]. The concentrations of  $M_2$ ,  $M_3$ ,  $M_4$ ,  $M_5$ ,  $M_6$  slightly increased and reached saturation after day 150

$$\Delta G = \Delta H - T\Delta S. \quad (7)$$

The saturation of the A $\beta$  concentration indicates that the amount of A $\beta$  that can dissolve in the brain reaches the maximum. When the A $\beta$  concentration saturation, it aggregates to form plaques in the brain [38]. A $\beta$  plaques have a denser structure, making them difficult to clear.

Moreover, for  $M_2$ ,  $M_3$ ,  $M_4$ ,  $M_5$ ,  $M_6$ , and  $O$ , the A $\beta$  concentration significantly increased from day 0 to day 90, then increased slowly until day 150 and stabilized until day 180. The concentration of the fibrils ( $P$ ) increased until day 180 because the fibrils tended to be more stable and more difficult to break down than the other A $\beta$  structures. Therefore, the concentration of fibrils tends to increase in the brain over time.

Table 4 shows the A $\beta$  growth concentration values over 180 days at intervals of 30 days. According to Table 4, there was a difference in the concentrations of A $\beta$  in  $M_2$ ,  $M_3$ ,  $M_4$ ,  $M_5$ ,  $M_6$ , and  $O$  on the same day. This

**Table 4:** The values of the A $\beta$  concentration over 180 days

Concentration (g mL <sup>-1</sup> )	Days to-						
	0	30	60	90	120	150	180
$M_1$	0	73.828	73.828	73.828	73.828	73.828	73.828
$M_2$	0	9.864	13.146	14.231	14.589	14.707	14.746
$M_3$	0	1.819	2.699	2.991	3.088	3.120	3.130
$M_4$	0	0.269	0.419	0.469	0.485	0.491	0.493
$M_5$	0	0.114	0.183	0.206	0.214	0.216	0.217
$M_6$	0	0.022	0.036	0.040	0.042	0.042	0.042
$O$	0	0.011	0.018	0.020	0.021	0.021	0.021
$P$	0	1.006	4.317	8.546	13.079	17.710	22.373

demonstrates that the growth concentrations of  $M_1$ ,  $M_2$ ,  $M_3$ ,  $M_4$ ,  $M_5$ ,  $M_6$ , and  $O$  increase daily over the course of 180 days, but the difference in concentration between  $M_1$ ,  $M_2$ ,  $M_3$ ,  $M_4$ ,  $M_5$ ,  $M_6$ , and  $O$  decreases at the same time.

The kinetic process of A $\beta$  begins with A $\beta$  monomers, which are normal products of APP cleavage. Monomers have the potential to undergo association through noncovalent interactions. Subsequently, the monomers undergo the nucleation phase, which involves a critical concentration of monomers for nucleus formation. The initiation point of nucleation starts with the formation of nuclei, which serve the purpose of forming small aggregates. Once the nuclei are formed, A $\beta$  monomers will continue to undergo aggregation until oligomers are formed [39].

Oligomers can evolve into protofibrils with larger structures. Protofibrils represent the transitional phase between oligomers and fibrils. Subsequently, protofibrils undergo an elongation phase in which they elongate and aggregate to form fibrils. The fibrils then continue to accumulate, forming A $\beta$  plaques [6,17,37].

In the nucleation phase, there are sometimes two types of cleavage: primary nucleation and secondary nucleation. Primary nucleation refers to the formation of A $\beta$  from monomers without the involvement of preexisting aggregates. Moreover, secondary nucleation involves preexisting aggregates. Generally, preexisting fibrils can act as seeds for the aggregation of new monomers. Secondary nucleation is a process that can accelerate the growth of A $\beta$  fibrils and is more efficient [29,35,41].

Thermodynamically, secondary nucleation is more favorable and occurs spontaneously than primary nucleation. During secondary nucleation, preexisting aggregates act as templates, reducing the activation energy and facilitating the formation of new nuclei. Conversely, the formation of nuclei during primary nucleation involves the assembly of monomers into aggregates. This process requires a significant amount of energy, making it less favorable and not occurring spontaneously [5,21].

### 3.2 Simulation results for the immune system

The immune system within the brain includes microglia and astrocytes. Figure 3 shows a comparison of the concentration of A $\beta$  in the A $\beta$  growth models without the immune system and with the immune system.

As shown in Figure 3, the effect of the immune system on the A $\beta$  growth model showed a pattern of concentration increase similar to that of the model without the immune system. However, the concentrations calculated for the immune system were lower. This indicates that the abilities of microglia and astrocytes, which are involved in the immune system, play a role in reducing A $\beta$  accumulation. The role of the immune system becomes apparent from the growth of dimers ( $M_2$ ) to fibrils ( $P$ ). This is expected to bring the concentration of A $\beta$  growth from the dimers to the fibrils back to the initial monomeric form. Compared with those in the model without the immune system, the concentrations of A $\beta$  generated by  $M_2$ ,  $M_3$ ,  $M_4$ ,  $M_5$ ,  $M_6$ ,  $O$  (oligomer), and  $P$  (fibril) were significantly lower.

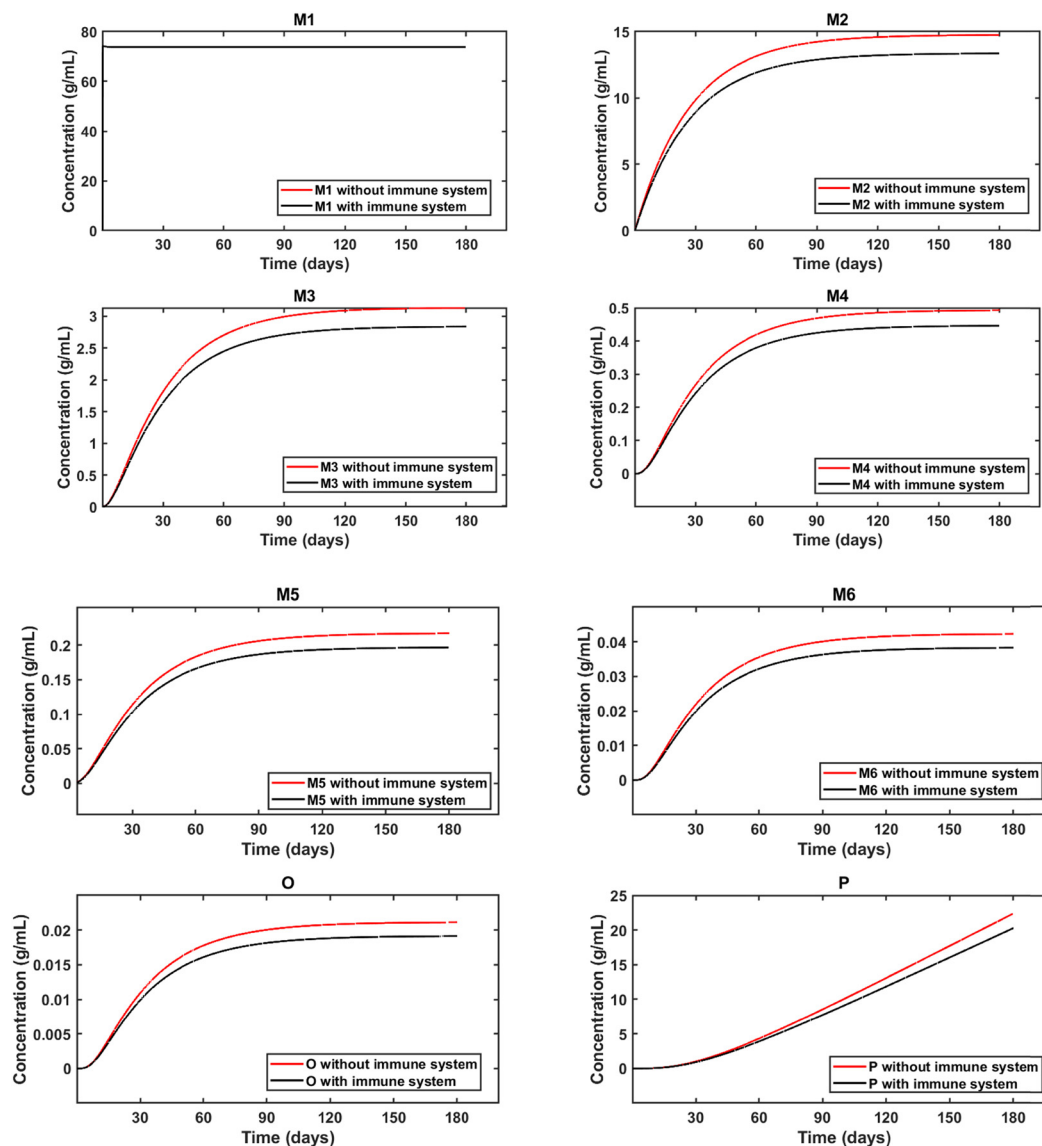


**Figure 3:** Comparison of A $\beta$  growth concentration values ( $\text{g mL}^{-1}$ ) without the immune system (red line) and with the immune system (black line) for each of  $M_1$ ,  $M_2$ ,  $M_3$ ,  $M_4$ ,  $M_5$ ,  $M_6$ ,  $O$ , and  $P$  over 180 days.

Table 5 shows the changes in the A $\beta$  concentration with the involvement of the immune system. There was a difference in the change in A $\beta$  concentration with the immune system compared to without the immune system over 180 days. A difference in the change in the A $\beta$  concentration was observed at the saturation state on day 180. This is because A $\beta$  growth has reached a point where there is no further accumulation. The difference in the change in concentration for each form is  $1.389 \text{ g mL}^{-1}$  for  $M_2$ ,  $0.295 \text{ g mL}^{-1}$  for  $M_3$ ,  $0.046 \text{ g mL}^{-1}$  for  $M_4$ ,  $0.020 \text{ g mL}^{-1}$  for  $M_5$ ,  $0.004 \text{ g mL}^{-1}$  for  $M_6$ ,  $0.002 \text{ g mL}^{-1}$  for  $O$ , and  $2.110 \text{ g mL}^{-1}$  for  $P$ .

Most A $\beta$  peptides can be soluble in brain fluid, especially in the form of monomers or small oligomers. Under normal conditions, A $\beta$  peptides are cleared through two mechanisms: the enzymatic pathway and the nonenzymatic pathway. The nonenzymatic pathway includes phagocytosis by microglia in small quantities and transport across the *blood–brain barrier*. Conversely, enzymatic clearance involves several proteases such as neprilysin and *insulin-degrading enzyme*, which play a role in breaking down A $\beta$  into smaller fragments, allowing it to dissolve in the extracellular fluid [40,43]. However, A $\beta$  peptides can become insoluble, leading to aggregation and the formation of plaques composed of larger fibrils.

**Table 5:** The concentration of A $\beta$  increased with the involvement of the immune system over 180 days

Concentration (g mL <sup>-1</sup> )	Days to-						
	0	30	60	90	120	150	180
$M_1$	0	73.828	73.828	73.828	73.828	73.828	73.828
$M_2$	0	8.933	11.907	12.890	13.214	13.321	13.357
$M_3$	0	1.647	2.445	2.709	2.797	2.826	2.835
$M_4$	0	0.243	0.379	0.425	0.440	0.445	0.446
$M_5$	0	0.103	0.166	0.187	0.193	0.196	0.196
$M_6$	0	0.020	0.032	0.036	0.038	0.038	0.038
$O$	0	0.010	0.016	0.018	0.019	0.019	0.019
$P$	0	0.910	3.909	7.739	11.844	16.039	20.263

The accumulation of A $\beta$  in Alzheimer's patients leads to inflammation in the brain, activating astrocytes and microglia, which then produce proinflammatory cytokines that damage neurons. If not addressed, more damaged and dead neurons will accumulate, disrupting communication pathways and cognitive functions. This is due to apoptosis, a programmed cell death process. Proinflammatory cytokines such as TNF- $\alpha$  trigger apoptosis, causing the gradual death of neurons [2,27].

Anti-inflammatory cytokines can regulate the immune system to stimulate microglia and macrophages to clear A $\beta$  plaques. Macrophages, which exhibit phagocytic properties, engulf A $\beta$  particles. The concentration of A $\beta$  in growing plaques decreases over time. If the number of A $\beta$  plaques decreases, inflammation will also decrease, allowing for the resolution of neuronal death.

The ability of microglia to clear A $\beta$  plaques is influenced by several factors such as the concentration of A $\beta$  oligomers, microglial performance, and individual variability. The greater the concentration of A $\beta$  oligomers in the brain is, the longer it may take for microglia to clear A $\beta$  plaques. Age can affect the performance of microglia, potentially slowing the clearance process. Other factors such as genetics and overall health can impact the efficiency of microglia as antibodies [22].

### 3.3 Simulation results of drug therapy

One approach to addressing Alzheimer's disease is through drug therapy. Drug therapy involving the immune system is used to simulate the formation of dimers ( $M_2$ ) to fibrils ( $P$ ). The rationale is similar to the application in the immune system, aiming to reduce the concentration of dimer to fibril growth in A $\beta$  back to the monomeric form.

The drug therapy used involves anti-A $\beta$  medications. As shown in Figure 4, the effect of drug therapy on the A $\beta$  growth model showed a pattern of concentration increase similar to that of the immune system model and the model without the immune system. However, the concentrations calculated for drug therapy were lower than those for the immune system and the model without the immune system. This finding indicates that the effectiveness of anti-A $\beta$  drugs is an effective therapeutic approach for reducing A $\beta$  plaque growth.

Table 6 shows the concentrations of A $\beta$  increased with the use of a combination of drugs and the immune system. According to Table 6, the A $\beta$  concentration significantly decreased compared to the concentrations in the previous model, especially the fibril concentration. There was a difference in the change in the A $\beta$  concentration between patients who did and did not receive drug therapy over 180 days. A difference in the change in the A $\beta$  concentration was observed at the saturation state on day 180. This is because A $\beta$  growth has reached a point where there is no further accumulation. The difference in the change in concentration for each form was 4.343 g mL<sup>-1</sup> for  $M_2$ , 0.922 g mL<sup>-1</sup> for  $M_3$ , 0.145 g mL<sup>-1</sup> for  $M_4$ , 0.064 g mL<sup>-1</sup> for  $M_5$ , 0.012 g mL<sup>-1</sup> for  $M_6$ , 0.006 g mL<sup>-1</sup> for  $O$ , and 6.594 g mL<sup>-1</sup> for  $P$ .

Drug therapy for Alzheimer's disease mainly involves inhibiting A $\beta$  aggregation. The drug used in this study was Aducanumab. Aducanumab is an anti-A $\beta$  drug classified as immunoglobulin type 1 (IgG1). Anti-A $\beta$

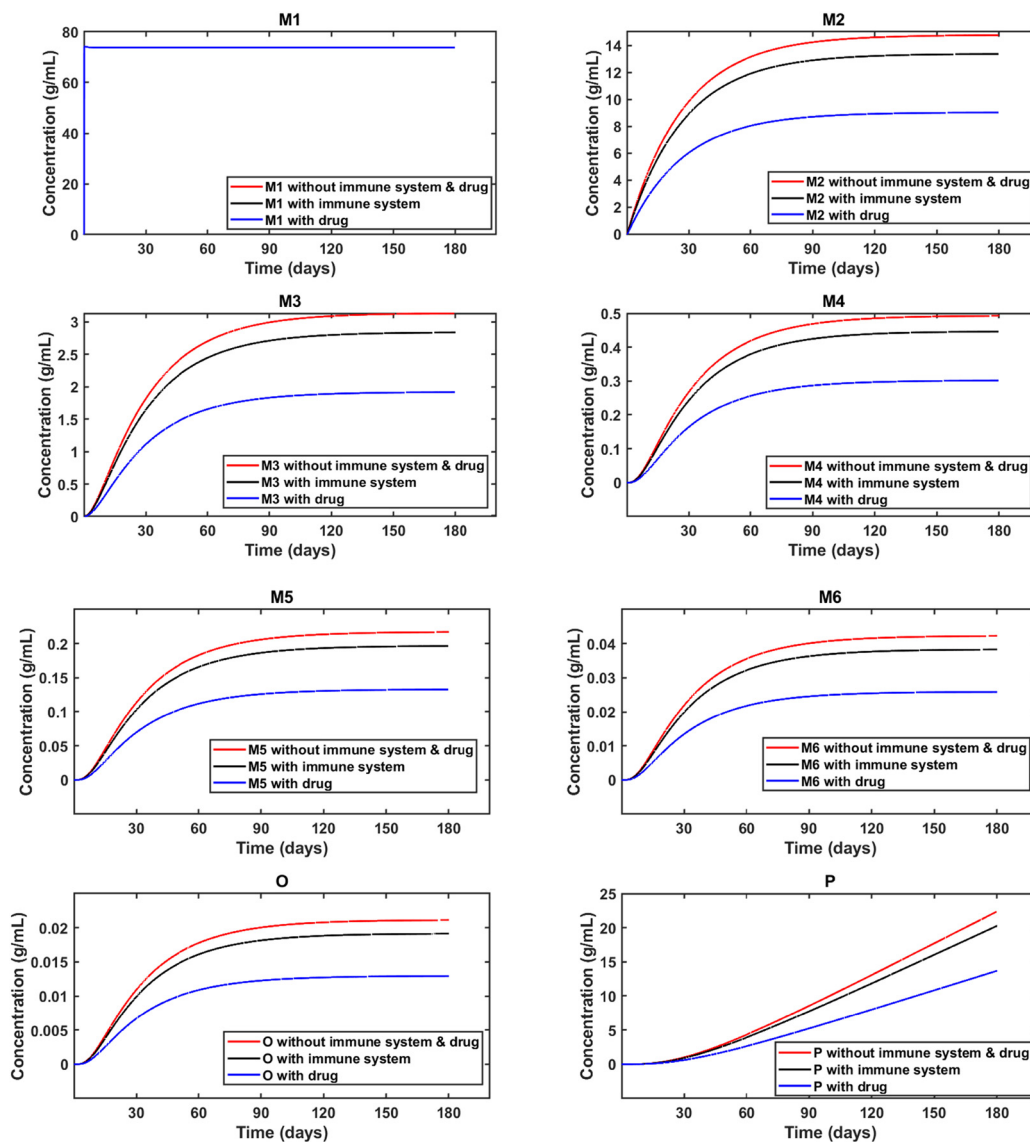


**Figure 4:** Comparison of A $\beta$  growth concentration values ( $\text{g mL}^{-1}$ ) without the immune system and drug (red line), with the immune system (black line), and with a combination of drugs and immune system (blue line) for each of  $M_1$ ,  $M_2$ ,  $M_3$ ,  $M_4$ ,  $M_5$ ,  $M_6$ ,  $O$ , and  $P$  over 180 days.

**Table 6:** The concentration of A $\beta$  increased with the use of a combination of drugs and the immune system over 180 days

Concentration ( $\text{g mL}^{-1}$ )	Days to-						
	0	30	60	90	120	150	180
$M_1$	0	73.828	73.828	73.828	73.828	73.828	73.828
$M_2$	0	6.953	9.273	10.039	10.292	10.376	10.404
$M_3$	0	1.281	1.904	2.110	2.179	2.201	2.209
$M_4$	0	0.189	0.295	0.331	0.342	0.346	0.347
$M_5$	0	0.080	0.129	0.145	0.151	0.152	0.153
$M_6$	0	0.015	0.025	0.028	0.029	0.030	0.030
$O$	0	0.008	0.013	0.014	0.015	0.015	0.015
$P$	0	0.707	3.041	6.024	9.221	12.489	15.779

drugs aim to reduce the formation of toxic A $\beta$  oligomers and enhance the clearance of A $\beta$  from the brain [25]. These drugs work by targeting specific molecular mechanisms, such as primary nucleation, secondary nucleation, and concentration-dependent aggregation of monomers [1].

Anti-A $\beta$  drugs selectively target A $\beta$  aggregates, including A $\beta$  plaques and oligomers, but do not target A $\beta$  monomers. This is because, in the aggregation process, A $\beta$  has a high energy barrier for the transition state [36]. Oligomers are believed to be more toxic form than fibril assemblies [13]. As a result, Aducanumab binds to A $\beta$  plaques and oligomers and then stimulates microglia to reduce A $\beta$ . The effectiveness of anti-A $\beta$  drug therapy can reduce the rate of Alzheimer's disease decline by approximately 30% and has a significant impact on disease progression [33]. The dosage and duration of treatment significantly influence the effectiveness of anti-A $\beta$  drugs in slowing cognitive impairment.

### 3.4 Determining the duration of treatment

The duration of treatment can be determined from Figure 4. Figure 4, shows that the A $\beta$  concentration begins to increase from day 120 to day 180. The saturation values in the context of drug usage imply that the frequency of drug administration is no longer capable of significantly increasing therapeutic effectiveness. The effectiveness of drug therapy in this case refers to the ability to reduce the concentration of A $\beta$ .

According to Honig and Boyd [16], in controlled trials, the typical duration of treatment is approximately 6 months, at which point the drug has provided significant benefits. The simulation results for determining the duration of treatment confirmed the reference, which is approximately 4 months starting from day 0 to 120th days. However, the duration of treatment for Alzheimer's patients is influenced by several factors such as age, the patient's condition, and the A $\beta$  concentration. The findings regarding the treatment duration can provide insights for further research on developing more effective drugs. Until now, the use of anti-A $\beta$  drug therapy has only been able to reduce the concentration of A $\beta$  but has not been able to completely clear A $\beta$  from the brain [45].

The ideal duration of treatment depends on the specific condition of the patient. According to Osborne and Schenk, the average duration of drug availability for Alzheimer's disease patients ranges from 31 weeks until 243 weeks [9,32,36].

### 3.5 Simulation results of the concentration rate

The growth concentration rate indicates the kinetics of changes that can indicate how fast or slow A $\beta$  growth is. Figure 5 shows the comparison of the rate of increase in the A $\beta$  concentration with the immune system, drug therapy, and the absence of both agents. All three simulation models exhibit patterns of increasing and decreasing rates on the same days. However, based on Figure 5, it is evident that the concentration of A $\beta$  in the context of drug therapy decreased compared to that in the immune system and in the absence of both agents.

A significant difference in the A $\beta$  concentration was detected in  $M_2$ . This is due to the difference in the structure between A $\beta$  monomers and dimers ( $M_2$ ). Structural differences can influence the A $\beta$  growth concentration rate significantly by impacting how quickly dimers are formed [23]. A $\beta$  dimers result from the aggregation of monomeric forms, increasing the density of dimers. Denser dimers tend to join other A $\beta$  molecules more quickly, triggering an increase in the concentration. Additionally, the availability of A $\beta$  monomers also affects the concentration of  $M_2$ . When the concentration of A $\beta$  monomers is very high, dimer formation increases, thereby increasing the rate of dimer formation.

At high concentrations, A $\beta$  will interact with each other through chemical interactions to form aggregates with large molecular weights that are capable of producing larger aggregates. These aggregates are the precursors to fibril growth. The ability of monomers to aggregate also influences the concentration rate [28]. Therefore, the curve of trimer ( $M_3$ ) to oligomer ( $O$ ) has different points of maximum rate increase due to the presence of a critical concentration that triggers the aggregation process [31]. If the formed nucleus is the same size, then in the nucleation stage, the aggregation rate will tend to be uniform [30].

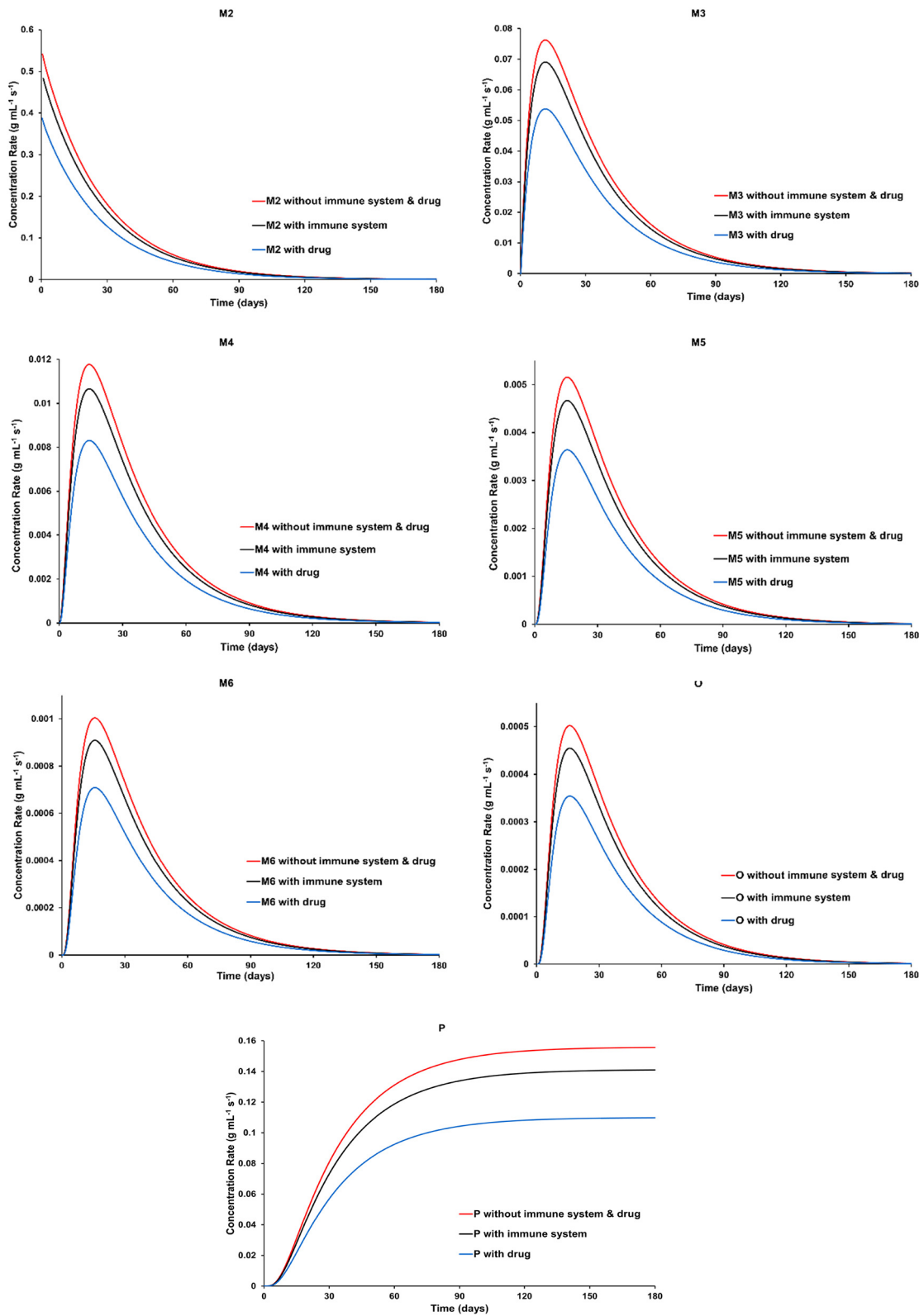


**Figure 5:** Comparison of the growth concentration rates (g mL<sup>-1</sup> s<sup>-1</sup>) of A $\beta$  without the immune system and drug (red line), with the immune system (black line), and with a combination of drugs and the immune system (blue line) for each of  $M_2$ ,  $M_3$ ,  $M_4$ ,  $M_5$ ,  $M_6$ ,  $O$ , and  $P$  over 180 days.



## 4 Conclusions

The development of an Alzheimer's disease model through computation can provide insights into the dynamics and kinetics of Alzheimer's. The dynamics and kinetics of A $\beta$  aggregation involve numerous processes, including primary nucleation, secondary nucleation, and elongation. In the dynamics of Alzheimer's disease model development, there is a complexity in the pathological progression that involves the accumulation of A $\beta$  plaques, inflammation, and synaptic damage over time. Meanwhile, the kinetics of Alzheimer's describes the factors influencing the development of Alzheimer's disease, such as the accumulation of A $\beta$  protein, the immune system response, and the response to drug therapy.

The initial concentration of the A $\beta$  monomer and its ability to aggregate are factors that influence the rate of A $\beta$  release. The relationship between growth concentration and aggregation indicates that an increase in A $\beta$  concentration can enhance the potential for aggregation. Conversely, an increase in A $\beta$  aggregation can lead to greater accumulation, thereby increasing the A $\beta$  concentration.

Simulations of A $\beta$  growth involving the immune system and drug therapy have shown that the use of a combination of drugs and the immune system influences the A $\beta$  concentration, thus capable of slowing the aggregation process. Currently, drug therapy has not been able to completely eliminate A $\beta$  in the brain. This indicates that the available drugs still need further development.

The effective duration of drug treatment based on simulation results is approximately 4 months starting from the time the drug was first administered. This is because the administered drug is no longer able to provide a significant effect. The determination of the treatment duration depends on the patient's condition. The longer the treatment is, the more likely it is to result in side effects, resistance, and a reduction in the benefits of the drug.

**Funding information:** Authors state no funding involved.

**Author contributions:** Cindyawati Cindyawati, Faozan Ahmad, and Agus Kartono conceived the idea, conducted analyses and simulation, and drafted the manuscript. Hendradi Hardhienata conceptualized the flow for the entire manuscript draft, verified all the results, and edited the draft.

**Conflict of interest:** There are no conflicts of interest to declare. The authors have no competing interests.

**Code availability:** Not applicable, formulas can be coded using any programming platform.

**Ethical approval:** This research did not require ethical approval.

## References

- [1] M. Bartolini, C. Bertucci, M. L. Bolognesi, A. Cavalli, C. Melchiorre, & V. Andrisano. (2007). Insight into the kinetic of amyloid  $\beta$  (1-42) peptide self-aggregation: Elucidation of inhibitors' mechanism of action. *ChemBioChem*, 8(17), 2152–2161. doi: 10.1002/cbic.200700427.
- [2] G. Bieri, K. M. Lucin, C. E. O'Brien, H. Zhang, S. A. Villeda, & T. Wyss-Coray, (2018). Proteolytic cleavage of Beclin 1 exacerbates neurodegeneration. *Molecular Neurodegeneration*, 13(1), 1–19. doi: 10.1186/s13024-018-0302-4.
- [3] A. K. Buell. (2022). Stability matters, too – the thermodynamics of amyloid fibril formation. *Chemical Science*, 13(35), 10177–10192. doi: 10.1039/d1sc06782f.
- [4] S. Burgold, S. Filser, M. M. Dorostkar, B. Schmidt, & J. Herms. (2014). In vivo imaging reveals sigmoidal growth kinetic of  $\beta$ -amyloid plaques. *Acta Neuropathologica Communications*, 2(1), 1–11. doi: 10.1186/2051-5960-2-30.
- [5] E. Chatani, & N. Yamamoto. (2017). Recent progress on understanding the mechanisms of amyloid nucleation. *Biophysical Reviews*, 10(2), 527–534. doi: 10.1007/s12551-017-0353-8.
- [6] G. F. Chen, T. H. Xu, Y. Yan, Y. R. Zhou, Y. Jiang, K. Melcher, H. Eric Hu. (2017). Amyloid beta: Structure, biology and structure-based therapeutic development. *Acta Pharmacologica Sinica*, 38(9), 1205–1235. doi: 10.1038/aps.2017.28.

- [7] S. I. A. Cohen, M. Vendruscolo, C. M. Dobson, & T. P. J. Knowles. (2012). From macroscopic measurements to microscopic mechanisms of protein aggregation. *Journal of Molecular Biology*, 421(2–3), 160–171. doi: 10.1016/j.jmb.2012.02.031.
- [8] D. L. Craft, L. M. Wein, & D. J. Selkoe. (2002). A mathematical model of the impact of novel treatments on the A $\beta$  burden in the Alzheimer's brain, CSF and plasma. *Bulletin of Mathematical Biology*, 64(5), 1011–1031. doi: 10.1006/bulm.2002.0304.
- [9] J. Cummings, G. Lee, A. Ritter, & K. Zhong. (2018). Alzheimer's disease drug development pipeline: 2018. *Alzheimer's & Dementia: Translational Research & Clinical Interventions*, 4(2018), 195–214. doi: 10.1016/j.trci.2018.03.009.
- [10] J. Cummings, & S. Salloway. (2021). Aducanumab: Appropriate use recommendations. *Alzheimer's & dementia : the journal of the Alzheimer's Association*, 18(3), 1–3. doi: 10.1002/alz.12444.
- [11] A. Fani Maleki, & S. Rivest. (2019). Innate immune cells: Monocytes, monocyte-derived macrophages and microglia as therapeutic targets for Alzheimer's disease and multiple sclerosis. *Frontiers in Cellular Neuroscience*, 13, 1–8. doi: 10.3389/fncel.2019.00355.
- [12] P. E. Fraser, L. K. Duffy, M. B. O'Malley, J. Nguyen, H. Inouye, & D. A. Kirschner. (1991). Morphology and antibody recognition of synthetic  $\beta$ -amyloid peptides. *Journal of Neuroscience Research*, 28(4), 474–485. doi: 10.1002/jnr.490280404.
- [13] S. Giorgetti, C. Greco, P. Tortora, & F. A. Aprile. (2018). Targeting amyloid aggregation: An overview of strategies and mechanisms. *International Journal of Molecular Sciences*, 19(9). doi: 10.3390/ijms19092677.
- [14] W. Hao, & A. Friedman. (2016). Mathematical model on Alzheimer's disease. *BMC Systems Biology*, 10(1), 1–18. doi: 10.1186/s12918-016-0348-2.
- [15] S. E. Hill, J. Robinson, G. Matthews, & M. Muschol. (2009). Amyloid protofibrils of lysozyme nucleate and grow via oligomer fusion. *Biophysical Journal*, 96(9), 3781–3790. doi: 10.1016/j.bpj.2009.01.044.
- [16] L. S. Honig, & C. D. Boyd. (2013). Treatment of Alzheimer's disease: Current management and experimental therapeutics. *Current Translational Geriatrics and Experimental Gerontology Reports*, 2(3), 174–181. doi: 10.1007/s13670-013-0056-3.
- [17] M. Hoshino. (2017). Fibril formation from the amyloid- $\beta$  peptide is governed by a dynamic equilibrium involving association and dissociation of the monomer. *Biophysical Reviews*, 9(1), 9–16. doi: 10.1007/s12551-016-0217-7.
- [18] Y. R. Huang, & R. T. Liu. (2020). The toxicity and polymorphism of  $\beta$ -amyloid oligomers. *International Journal of Molecular Sciences*, 21(12), 1–19. doi: 10.3390/ijms21124477.
- [19] C. R. Jack Jr, H. J. Wiste, T. G. Lesnick, S. D. Weigand, D. S. Knopman, P. Vemuri ... R. C. Petersen. (2013). Brain  $\beta$ -amyloid load approaches a plateau. *Neurology*, 80(10), 890–896. doi: 10.1212/WNL.0b013e3182840bbe.
- [20] T. P. J. Knowles, C. A. Waudby, G. L. Devlin, S. I. A. Cohen, A. Aguzzi, M. Vendruscolo ... C. M. Dobson. (2009). An analytical solution to the kinetics of breakable filament assembly. *Science*, 326(5959), 1533–1537. doi: 10.1126/science.1178250.
- [21] S. Kumar, & J. Walter. (2011). Phosphorylation of amyloid beta peptides. *Aging (Albany NY)*, 3(8), 803–812. doi: 10.18632/aging.100362.
- [22] C. Y. D. Lee, & G. E. Landreth. (2010). The role of microglia in amyloid clearance from the AD brain. *Journal of Neural Transmission*, 117(8), 949–960. doi: 10.1007/s00702-010-0433-4.
- [23] M. R. Lindstrom, M. B. Chavez, E. A. Gross-Sable, E. Y. Hayden, & D. B. Teplow. (2021). From reaction kinetics to dementia: A simple dimer model of Alzheimer's disease etiology. *PLoS Computational Biology*, 17(7), 1–24. doi: 10.1371/journal.pcbi.1009114.
- [24] S. Linse. (2017). Monomer-dependent secondary nucleation in amyloid formation. *Biophysical Reviews*, 9(4), 329–338. doi: 10.1007/s12551-017-0289-z.
- [25] S. Linse. (2019). Mechanism of amyloid protein aggregation and the role of inhibitors. *Pure and Applied Chemistry*, 91(2), 211–229. doi: 10.1515/pac-2018-1017.
- [26] A. Lomakin, D. B. Teplow, D. A. Kirschner, & G. B. Benedek. (1997). Kinetic theory of fibrillogenesis of amyloid  $\beta$ -protein. *Proceedings of the National Academy of Sciences of the United States of America*, 94(15), 7942–7947. doi: 10.1073/pnas.94.15.7942.
- [27] S. López-Ortiz, J. Pinto-Fraga, P. L. Valenzuela, J. Martín-Hernández, M. M. Seisdedos, O. García-López ... A. Santos-Lozano. (2021). Physical exercise and Alzheimer's disease: Effects on pathophysiological molecular pathways of the disease. *International Journal of Molecular Sciences*, 22(6), 1–29. doi: 10.3390/ijms22062897.
- [28] V. H. Man, X. He, B. Ji, S. Liu, X. Q. Xie, & J. Wang. (2019). Molecular mechanism and kinetics of amyloid- $\beta$ 42 aggregate formation: a simulation study. *ACS Chemical Neuroscience*, 10(11), 4643–4658. doi: 10.1021/acschemneuro.9b00473.
- [29] G. Meisl, X. Yang, E. Hellstrand, B. Frohm, J. B. Kirkegaard, S. I. Cohen ... T. P. J. Knowles. (2014). Differences in nucleation behavior underlie the contrasting aggregation kinetics of the A $\beta$ 40 and A $\beta$ 42. *Proceedings of the National Academy of Sciences*, 111(26), 9384–9389. doi: 10.1073/pnas.1401564111.
- [30] S. Nag, B. Sarkar, A. Bandyopadhyay, B. Sahoo, V. K. A. Sreenivasan, M. Kombrabail ... S. Maiti. (2011). Nature of the amyloid- $\beta$  monomer and the monomer-oligomer equilibrium. *Journal of Biological Chemistry*, 286(16), 13827–13833. doi: 10.1074/jbc.M110.199885.
- [31] M. Novo, S. Freire, & W. Al-Soufi. (2018). Critical aggregation concentration for the formation of early Amyloid- $\beta$  (1–42) oligomers. *Scientific Reports*, 8(1), 3–10. doi: 10.1038/s41598-018-19961-3.
- [32] O. M. Osborne, O. Naranjo, B. L. Heckmann, D. Dykxhoorn, & M. Toborek. (2023). Anti-amyloid: An antibody to cure Alzheimer's or an attitude. *iScience*, 26(8), 107461. doi: 10.1016/j.isci.2023.107461.
- [33] A. Salehipour, M. Bagheri, M. Sabahi, M. Dolatshahi, & D. Boche. (2022). Combination therapy in Alzheimer's disease: Is it time?. *Journal of Alzheimer's Disease*, 87(4), 1433–1449. doi: 10.3233/JAD-215680.
- [34] B. Sarkar, A. K. Das, & S. Maiti. (2013). Thermodynamically stable amyloid- $\beta$  monomers have much lower membrane affinity than the small oligomers. *Frontiers in Physiology*, 4(1–11). doi: 10.3389/fphys.2013.00084.

- [35] T. Scheidt, U. Łapińska, J. R. Kumita, D. R. Whiten, D. Klenerman, M. R. Wilson ... P. Arosio. (2019). Secondary nucleation and elongation occur at different sites on Alzheimer's amyloid- $\beta$  aggregates. *Science Advances*, 5(4), 1. doi: 10.1126/sciadv.aau3112.
- [36] D. Schenk, G. S. Basi, & M. N. Pangalos. (2012). Treatment strategies targeting amyloid-protein. *Cold Spring Harbor Perspectives in Medicine*, 2, 1–33. doi: 10.1101/cshperspect.a006387.
- [37] J. D. Schmit, K. Ghosh, & K. Dill. (2011). What drives amyloid molecules to assemble into oligomers and fibrils?. *Biophysical Journal*, 100(2), 450–458. doi: 10.1016/j.bpj.2010.11.041.
- [38] U. Sengupta, A. N. Nilson, & R. Kaye. (2016). The role of amyloid- $\beta$  oligomers in toxicity, propagation, and immunotherapy. *EBioMedicine*, 6(42–49). doi: 10.1016/j.ebiom.2016.03.035.
- [39] X. Sun, W. D. Chen, & Y. D. Wang. (2015).  $\beta$ -Amyloid: The key peptide in the pathogenesis of Alzheimer's disease. *Frontiers in Pharmacology*, 6, 221. doi: 10.3389/fphar.2015.00221.
- [40] J. M. Tarasoff-Conway, R. O. Carare, R. S. Osorio, L. Glodzik, T. Butler, E. Fieremans ... M. J. de Leon. (2015). Clearance systems in the brain – Implications for Alzheimer disease. *Nature Reviews Neurology*, 11(8), 457–470. doi: 10.1038/nrneurol.2015.119.
- [41] D. Thacker, M. Barghouth, M. Bless, E. Zhang, & S. Linse. (2023). Direct observation of secondary nucleation along the fibril surface of the amyloid  $\beta$  42 peptide. *Proceedings of the National Academy of Sciences of the United States of America*, 120(25), 1–9. doi: 10.1073/pnas.2220664120.
- [42] W. Y. Wang, M. S. Tan, J. T. Yu, & L. Tan. (2015). Role of pro-inflammatory cytokines released from microglia in Alzheimer's disease. *Annals of Translational Medicine*, 3(10), 1–15. doi: 10.3978/j.issn.2305-5839.2015.03.49.
- [43] K. R. Wildsmith, M. Holley, J. C. Savage, R. Skerrett, & G. E. Landreth. (2013). Evidence for impaired amyloid  $\beta$  clearance in Alzheimer's disease. *Alzheimer's Research & Therapy*, 5(4), 1–6. doi: 10.1186/alzrt187.
- [44] W. Yiming, S. J. Bunce, & S. E. Radford. (2018). Thermodynamic phase diagram of amyloid  $\beta$  (16–22) peptide. *Proceedings of the National Academy of Sciences*, 116(6), 2091–2096. doi: 10.1073/pnas.1819592116.
- [45] Y. Zhang, H. Chen, R. Li, K. Sterling, & W. Song. (2023). Amyloid  $\beta$ -based therapy for Alzheimer's disease: challenges, successes and future. *Signal Transduction and Targeted Therapy*, 8(1), 1–26. doi: 10.1038/s41392-023-01484-7.